WATER RESOURCES RESEARCH, VOL. 33, NO. 5, PAGES 1021–1033, MAY 1997

35

A model for numerical simulating of evaporation from bare saline soil

Alexander Yakirevich

Water Resources Research Center, J. Blaustein Institute for Desert Research, Ben-Gurion University of the Negev, Sede-Boker Campus, Israel

Pedro Berliner

Wyler Laboratory, J. Blaustein Institute for Desert Research, Ben-Gurion University of the Negev, Sede-Boker Campus, Israel

Shaul Sorek

Water Resources Research Center, J. Blaustein Institute for Desert Research, Ben-Gurion University of the Negev, Sede-Boker Campus, Israel

Abstract. A mathematical model for the computation of evaporation from bare saline soils is presented. Moisture flow and heat transport equations in the partially saturated zone of the soil are coupled at the soil surface with a lower atmosphere boundary layer model. The transport model considers multicomponent salt migration. The flow equation accounts for osmotic flux due to the presence of ion species in the soil solution. Nonlinear one-dimensional equations were solved using fully implicit finite difference schemes. The soil part of the model was tested using experimental data of water and solute redistribution under temperature gradients in sealed soil columns. In order to demonstrate the effect of soil salinity on the evaporation, the problem of water infiltration into soil with initially low water content and its subsequent evaporation was considered. Results show a significant effect of osmotic pressure gradients on predicted evaporation.

1. Introduction

Evaporation from the soil surface is controlled by atmospheric and soil conditions. Numerical models of soil water transport and energy balance may be used to describe this phenomena. Two approaches have been developed for coupling of soil water flow and heat transport in porous media. These are the "mechanistic" approach, based on the theory by *Philip and de Vries* [1957], and the thermodynamic approach, based on thermodynamics of irreversible processes [*Taylor and Cary*, 1965]. Critical surveys of different models, developed in recent years [e.g., *Sasamory*, 1970; *Sophocleous*, 1979; *Groenvelt and Kay*, 1974], and their applicability were carried out by many authors [e.g., *Milly*, 1982; *de Silans et al.*, 1989]. Coupling these models to the equations of the lower atmosphere boundary layer enables the estimation of evaporation and energy balance at the soil surface [e.g., *Schieldge et al.*, 1982; *Camillo et al.*, 1983]. *Scanlon* [1992] and *Scanlon and Milly* [1994] performed a detailed analysis concerning liquid and vapor fluxes in desert soils. Yet numerical models used in these and many of the above mentioned studies do not account for the influence of the salt concentration gradients on soil water flow. However, very close to the surface, in the soil zone affected by evaporation, the soil water films may be extremely thin. Under such conditions, salt concentration gradients can become a major factor affecting soil water movement [*Bresler et al.*, 1982].

Bresler and Laufer [1974] investigated effects of salt on water flow under conditions of relatively low water content. The results indicated that osmotic gradients and anion exclusion effects are of minor importance. However, both experiments and mathematical modeling were carried out under isothermal conditions for a two-phase system (solid and liquid). The authors suggested that in the more general case of a solid-liquid-gas system, the gas phase acts as a perfect membrane in a sense that it allows water vapor transfer but completely restricts the solute.

Conditions at the soil surface during the evaporation process maximize the effect of osmotic gradients on water flow [*Letey et al.*, 1969]. *Qayyum and Kemper* [1962] also presented experimental data that indicate that salt concentration gradients may modify the evaporation rate.

Nassar and Horton [1989b, 1992] developed a model to describe the simultaneous transfer of heat, water, and solute in the unsaturated zone of soil. This model was used for simulating water flow and salt transport under nonisothermal conditions in sealed soil columns. A good agreement between theory and experiments [*Nassar and Horton*, 1989a; *Nassar et al.*, 1992a, b] was obtained. It was shown that even in such a relatively simple system, solute concentration gradients affect soil water flow. Yet, the model of *Nassar and Horton* [1992] cannot be used in the presented form to evaluate evaporation. The flow equation is written in terms of water content and does not allow simulation in both the unsaturated and the saturated zones; only one component of salt was included in the transport model, and the hydraulic parameters were not dependent on soil salinity. However, as was shown by *Russo* [1988], effects of soil-matrix-soil solution (i.e., changes in the soil hydraulic properties, cation exchange, etc.) on the transient water flow may be of great significance.

Paper number 96WR03684.
0043-1397/97/96WR-03684$09.00

In what follows we present a new theoretical model of coupled soil water flow and heat and salt transport that includes osmotic pressure effects. This is then simulated numerically in order to estimate the relative influence of salt concentration gradients on evaporation from bare soil.

2. Model Description

The *Philip and de Vries* [1957] model describes soil water flow and heat transport in unsaturated-saturated soils. We modify this model to account for the osmotic part of the fluid flux induced by gradients of salt concentration.

The soil is considered a multiphase porous media domain composed of solid, liquid, and gas phases. The latter is a binary mixture of water vapor and dry air.

The following are the set of assumptions on which the model is based:

1. The solid matrix is undeformable and immobile.
2. Liquid water is incompressible, and its density does not depend on concentrations of dissolved constituents.
3. Hysteresis in the capillary pressure and hydraulic conductivity is neglected.
4. Water in the liquid phase and gas phases are in local thermodynamic equilibrium.
5. Flow in the liquid phase depends on gradients of matric potential, temperature, and salt concentration.
6. Water vapor behaves as a perfect gas, and its transport by advection is neglected.
7. Local thermal equilibrium exists among all phases.

The flux for the water component in the liquid phase is given by

$$\mathbf{q}_l = -\rho_l\left[K_l\left(\nabla\psi - \nabla z - \frac{\sigma'}{\rho_l g}\nabla P_{os}\right) + D_{Tl}\nabla T\right] \quad (1)$$

where $\mathbf{q}_l$ is the vector of mass flux of liquid water per unit area of porous medium, ψ is the matric pressure head, P_{os} is the osmotic pressure, T is the temperature, K_l is the hydraulic conductivity, D_{Tl} is the transport coefficient for adsorbed liquid flow due to temperature gradient, ρ_l is the density of liquid phase, σ' is the osmotic efficiency coefficient, g is gravity acceleration, and z is the vertical coordinate (positive downward).

The vector of mass vapor flux ($\mathbf{q}_v$) per unit area of porous medium is given by

$$\mathbf{q}_v = -D_v\nabla\rho_v \quad (2)$$

where D_v is an effective molecular diffusivity of water vapor, and ρ_v is the water vapor density.

When a local thermodynamic equilibrium exists between the water in the liquid and gas phases, the vapor density dependence on temperature and soil water potential was presented by *Edlefson and Anderson* [1943]. *Bresler et al.* [1982] suggested that the total potential is an additive function of matric and osmotic potentials. We can therefore write

$$\rho_v(\psi, P_{os}, T) = \rho_0(T)\exp\left(g\frac{\psi - P_{os}/\rho_l g}{RT}\right) \quad (3)$$

where ρ_0 is the saturation vapor density, and R is the gas constant for the water vapor.

Substitution of (3) into (2) yields

$$\mathbf{q}_v = -\rho_l\left\{\frac{gD_v\rho_v}{RT\rho_l}\nabla\left(\psi - \frac{P_{os}}{g\rho_l}\right) + \frac{D_v}{\rho_l}\cdot\left[\exp\left(g\frac{\psi - P_{os}/\rho_l g}{RT}\right)\frac{d\rho_0}{dT} - \frac{g\rho_v(\psi - P_{os}/\rho_l g)}{RT^2}\right]\nabla T\right\}$$
$$= -\rho_l[D_{\psi v}\nabla(\psi - P_{os}/\rho_l g) + D_{Tl}\nabla T] \quad (4)$$

where $D_{\psi v}$ and D_{Tv} are the isothermal and thermal vapor diffusivities. In view of (2) and (4), we write the total flux of water ($\mathbf{q}_m$) per unit area of porous medium:

$$\mathbf{q}_m = \mathbf{q}_l + \mathbf{q}_v = -\rho_l\left[(K_l + D_{\psi v})\nabla\psi - K_l\nabla z - \frac{1}{\rho_l g}(K_l\sigma' + D_{\psi v})\nabla P_{os} + (D_{Tl} + D_{Tv})\nabla T\right] \quad (5)$$

The total flux of sensible and latent heat is given by [*Milly*, 1982]

$$\mathbf{q}_h = -\lambda\nabla T - \rho_l(LD_{\psi v} + gTD_{Tl})\nabla\psi + c_l(T - T_0)\mathbf{q}_m \quad (6)$$

where λ is the effective thermal conductivity, L is the latent heat of vaporization of water, c_l is the specific heat of liquid water, and T_0 is a reference temperature.

The mass balance equation for the water components in the combined liquid and gas phase is given by

$$\frac{\partial}{\partial t}[\rho_l\theta + \rho_v(n - \theta)] = -\nabla\cdot\mathbf{q}_m \quad (7)$$

where n is the soil porosity, and θ is volumetric moisture content.

The energy balance equation of the combined solid, liquid, and gas phases is given by

$$\frac{\partial}{\partial t}[c_s\rho_s(1 - n) + c_l\rho_l\theta + c_p\rho_v(n - \theta) + L_0\rho_v(n - \theta)] = -\nabla\cdot\mathbf{q}_h \quad (8)$$

where ρ_s and c_s are the density and specific heat of solid phase, respectively; c_p is the specific heat of water vapor at constant pressure; and L_0 is the value of L at T_0. Note that we neglected the source term in the energy balance equation, (8), associated with the process of wetting, since it is significant only in preliminary stages of water infiltration into a very dry soil [*Bear et al.*, 1991].

In most cases, when simulating water flow and heat transport processes in unsaturated soil, the amount of water retained by soil is accepted as a function of matric potential and temperature [e.g., *Milly*, 1984]. However, water content is increased in soils with high smectite content as a result of the effect of concentration and composition of the soil solution [*McNeal and Coleman*, 1966; *Shainberg et al.*, 1971; *Russo and Bresler*, 1980]. It has been shown [*Pachepsky*, 1989] that in such a case the additional water retention may be expressed as a function of excessive thickness of hydrate-ion layers (HIL) in the interlayer spacing of smectite minerals. This excessive thickness (Δ) is the difference between the average thickness of HIL in minerals in the mixed Na-Ca form ($b_{\text{Na-Ca}}$) and minerals in Ca form (b_{Ca}), i.e. $\Delta = b_{\text{Na-Ca}} - b_{\text{Ca}}$. Thus, in this study we assume that liquid water content is a function of matric potential, temperature, and excessive thickness of HIL, that is, $\theta = \theta(\psi, T, \Delta)$.

Substitution of (5) into (7) yields the flow equation:

$$\left[\left(1-\frac{\rho_v}{\rho_l}\right)\frac{\partial\theta}{\partial\psi}+\frac{n-\theta}{\rho_l}\frac{\partial\rho_v}{\partial\psi}\right]\frac{\partial\psi}{\partial t}+\left[\left(1-\frac{\rho_v}{\rho_l}\right)\frac{\partial\theta}{\partial T}+\frac{n-\theta}{\rho_l}\frac{\partial\rho_v}{\partial T}\right]\frac{\partial T}{\partial t}+\left(1-\frac{\rho_v}{\rho_l}\right)\frac{\partial\theta}{\partial\Delta}\frac{\partial\Delta}{\partial t}+\frac{n-\theta}{\rho_l}\frac{\partial\rho_v}{\partial P_{os}}\frac{\partial P_{os}}{\partial T}=\nabla\cdot\left[(K_l+D_{\psi v})\nabla\psi-K_l\nabla z-\frac{1}{\rho_l g}(K_l\sigma'+D_{\psi v})\nabla P_{os}+(D_{Tl}+D_{Tv})\nabla T\right] \quad (9)$$

Substitution of (6) into (8) yields the heat transport equation:

$$\left[c_\lambda+L(n-\theta)\frac{\partial\rho_v}{\partial T}+\rho_v L\frac{\partial\theta}{\partial T}\right]\frac{\partial T}{\partial t}+\left[L(n-\theta)\frac{\partial\rho_v}{\partial\psi}-\rho_v L\frac{\partial\theta}{\partial\psi}+\right]\frac{\partial\psi}{\partial t}-\rho_v L\frac{\partial\theta}{\partial\Delta}\frac{\partial\Delta}{\partial t}+L(n-\theta)\frac{\partial\rho_v}{\partial P_{os}}\frac{\partial P_{os}}{\partial T}=\nabla\cdot[\lambda\nabla T+\rho_l(LD_{\psi v}+gTD_{Tl})\nabla\psi]-c_l\mathbf{q}_m\cdot\nabla T \quad (10)$$

in which $c_\lambda = c_s\rho_s(1-n)+c_l\rho_l\theta+c_p\rho_v(n-\theta)$.

The coupling of transport equations for different ion species with models of chemical equilibria, allows the simulation of multicomponent transport and reactions under transient flow conditions. Comprehensive review of such models are given by, for example, *Yeh and Tripathi* [1989] and *Simunek and Suarez* [1994]. Let us consider the following ions in the liquid phase: Ca^{2+}, Mg^{2+}, Na^+, H^+, Cl^-, SO_4^{2-}, OH^-, CO_3^{2-}, and HCO_3^-; cations on the exchange complex: Ca^{2+}, Mg^{2+}, and Na^+; and precipitated minerals on the solid phase: $CaSO_4 \times 2H_2O$ and $CaCO_3$. Denoting C_i (meq/L) as the total dissolved concentration of the ith component in the soil solution, where indices $i = 1, 2, 3, 4, 5$ correspond to Ca^{2+}, Mg^{2+}, Na^+, Cl^-, SO_4^{2-}, respectively, we can write the mass balance equation for each ith component in the form

$$\frac{\partial}{\partial t}[\theta C_i+(1-n)\rho_s(F_i^e+F_i^s)]=\nabla\cdot(D^*\theta\nabla C_i-\mathbf{q}_l'C_i) \quad (11)$$

where F_i^e is the mass of exchangeable ith cation per unit mass of the solid phase (meq/kg), F_i^s is the mass of precipitated ith component per unit mass of solid phase, D^* is the hydrodynamic dispersion coefficient (assumed to be the same for all ions), and $\mathbf{q}_l' = \mathbf{q}_l/\rho_l$ is the volumetric flux of water. The transport equation, (11), was coupled with the chemical equilibrium model LIBRA [*Platonova and Pachepsky*, 1989; *Pachepsky et al.*, 1993]. LIBRA includes the following processes: association of ions in the soil solution (the ion pairs formed are $CaCO_3^0$, $MgCO_3^0$, $NaCO_3^0$, $CaHCO_3^+$, $MgHCO_3^+$, $CaHCO_3^+$, $NaHCO_3^0$, $CaSO_4^0$, $MgSO_4^0$, $NaSO_4^-$, $CaOH^+$, $MgOH^+$, and $NaOH^0$); dissolution of CO_2 from the soil air; dissociation of carbonic acid and water; ion exchange between Ca^{2+}, Mg^{2+}, and Na^+; and dissolution-precipitation of gypsum and calcite. LIBRA simulates the equilibrium between salt components in soil solution, solid, and exchange phases. The equations describing mass and charge balance, complexation, and precipitation-dissolution reactions are similar to the ones presented by *Dufey et al.* [1979] and *Robbins et al.* [1980]. The LIBRA model does not use *Pitzer*'s [1979] relations to calculate activity coefficients at high ionic strength. Hence reliable results may be obtained when ionic strength of soil solution does not exceed 1 mol/L. Cation partition between the exchange phase and the solution is described by the Gapon equations [*Robbins et al.*, 1980]:

$$\frac{F_{Na}^e}{F_{Ca}^e}=K_{Na\text{-}Ca}\frac{a_{Na}}{(a_{Ca})^{1/2}} \qquad \frac{F_{Na}^e}{F_{Mg}^e}=K_{Na\text{-}Mg}\frac{a_{Na}}{(a_{Mg})^{1/2}} \quad (12)$$

where a_{Ca}, a_{Mg}, and a_{Na} are activities of Ca^{2+}, Mg^{2+}, and Na^+, respectively; and $K_{Na\text{-}Ca}$ and $K_{Na\text{-}Mg}$ are selectivity coefficients.

Note that we did not include in (11) the anion exclusion effect, since in laboratory experiments as well as numerical simulations it was shown that it can be neglected [*Bresler and Laufer*, 1974].

3. Initial and Boundary Conditions

In order to solve the set (9) to (11), initial and boundary conditions are needed. We consider the case of a one-dimensional (1-D) problem (in the vertical direction).

Initial conditions at the time t_0, describe the distributions in the soil profile of matric potential, temperature, ions, exchangeable cations and salt concentrations.

3.1. Boundary Conditions at the Soil Surface (z = 0)

The water flow equation, (9), is subject to a flux associated with the difference between prescribed rate of infiltration (Q) and computed rate of evaporation (E) through the soil surface, given by

$$-\rho_l\left[(K_l+D_{\psi v})\frac{\partial\psi}{\partial z}-K_l-\frac{1}{\rho_l g}(K_l\sigma'+D_{\psi v})\frac{\partial P_{os}}{\partial z}+(D_{Tl}+D_{Tv})\frac{\partial T}{\partial z}\right]=Q-E \quad (13)$$

The heat transport equation, (10), is subject to the condition

$$-\lambda\frac{\partial T}{\partial z}-\rho_l(LD_{\psi v}+gTD_{Tl})\frac{\partial\psi}{\partial z}+c_l(T-T_0)\mathbf{q}_m=G+c_lQT_l \quad (14)$$

where G denotes the heat flux into the soil and T_l denotes temperature of water infiltrating into soil.

The (i) ion components transport equation, (11), is subject to the following boundary condition:

$$-D^*\frac{\partial C_i}{\partial z}+\mathbf{q}_l'C_i=\mathbf{q}_l'C_{li} \qquad I=1,2,3,4,5 \quad (15)$$

where C_{li} is the ith ion concentration in water infiltrated through the soil surface.

In order to calculate values of E and G in (13) and (14), respectively, the water flow and heat transport equations in the soil are coupled with the low atmosphere boundary layer model [*Brutsaert*, 1982]:

$$R_{net}=H+LE+G \quad (16)$$

$$q_s-q_a=\frac{E}{ku^*\rho_d}\left[\ln\left(\frac{z_a}{z_0}\right)-\Omega_{EA}\right] \quad (17)$$

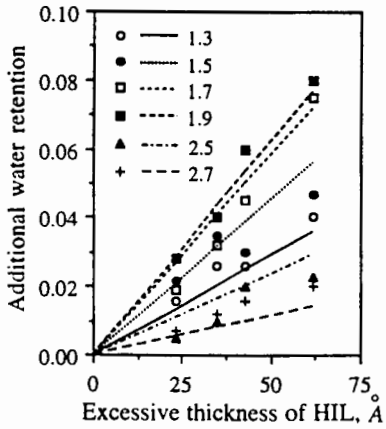

Figure 1. Additional water retention ($\delta\theta$) versus excessive thickness of HIL (Δ) for coarse loam soil (numbers are pF values): symbols represent the experimental data from *Russo and Bresler* [1980] as given by *Pachepsky* [1989]; lines represent the computed $\delta\theta$ using (25c) and (25d) for $\varphi_m = 0.00124$ Å^{-1}, $\omega = 1.86$, and $pF_m = 2.40$.

$$u_a = \frac{u^*}{k}\left[\ln\left(\frac{z_a}{z_0}\right) - \Omega_{UA}\right] \tag{18}$$

$$T_s - T_a = \frac{H}{ku^*\rho_d c_p}\left[\ln\left(\frac{z_a}{z_0}\right) - \Omega_{HA}\right] \tag{19}$$

where R_{net} is the net radiation flux; H is the sensible heat flux; q_s and q_a are the specific humidity of the air at height z_a and at the soil surface, respectively; u_a is the wind speed; u^* is the frictional velocity; T_a and T_s are the air temperature and the soil surface temperature, respectively; ρ_d is the dry air density; k is von Karman's constant; z_0 is the roughness length; and z_a is the height above the surface where the meteorological data are measured.

The diabatic correction functions Ω_{EA}, Ω_{HA}, and Ω_{UA} are given by the following expressions:
for unstable atmospheric conditions [*Brutsaert*, 1982].

$$\Omega_{EA} = \Omega_{HA} = 2\ln\left(\frac{1+x^2}{2}\right) \tag{20a}$$

$$\Omega_{UA} = 2\ln\left(\frac{1+x}{2}\right) + \ln\left(\frac{1+x^2}{2}\right) - 2\arctan(x) + \frac{\pi}{2} \tag{20b}$$

for stable atmospheric conditions [*de Silans et al.*, 1989],

$$\Omega_{EA} = \Omega_{HA} = \Omega_{UA} = -5z_a/L_{mo} \text{ for } 0 < z_a/L_{mo} \leq 1 \tag{20c}$$

$$\Omega_{EA} = \Omega_{HA} = \Omega_{UA} = -5[1 + \ln(z_a/L_{mo})] \text{ for } z_a/L_{mo} > 1 \tag{20d}$$

where $x = (1 - 16z_a/L_{mo})^{0.25}$ and L_{mo} is the Monin-Obukhov length, given by

$$L_{mo} = u_*^3\rho_d \Big/ kg\left(\frac{H}{T_a c_p} + 0.61E\right) \tag{21}$$

The net radiation heat flux is given by

$$R_{net} = S_R(1 - \alpha_s) + L_R - \varepsilon\sigma T_s^4 \tag{22}$$

where S_R is the prescribed incoming short wave radiation, α_s and ε are albedo and emissivity of the soil surface, σ is Stefan-Boltzman constant, T_s is the temperature of the soil surface, and L_R is long wave sky irradiance which is calculated following *Van Bavel and Hillel* [1976]:

$$L_R = \sigma(T_a + 273.16)^4[0.605 + 0.48(1370\rho_a)^{1/2}] \tag{23}$$

3.2. Conditions at the Lower Boundary ($z = z_b$)

Here we consider z_b to be far enough from groundwater level. Hence for the water flow and heat and solute transport equations, respectively, we write

$$\frac{\partial\psi}{\partial z} = 0 \qquad \frac{\partial T}{\partial z} = 0 \qquad \frac{\partial C_i}{\partial z} = 0 \qquad I = 1, 2, 3, 4, 5 \tag{24}$$

The boundary conditions (24) are given as an example and was then used in simulations. In the case in which groundwater level is situated close to the soil surface, any other appropriate boundary condition (Dirichlet, Neumann, or Cauchy type) can be used.

4. Model Parameters

The effect of temperature on matric potential is introduced as follows [*Milly*, 1984]:

$$\Psi(\theta) = \psi \exp[-C_\psi(T - T_0)] \tag{25a}$$

where $C_\psi \equiv 1/\psi\,\partial\psi/\partial T$ is a parameter assumed to be constant [*Milly*, 1984]. The variable Ψ is a temperature corrected potential, which is assumed to be a function of water content only. To describe the function $\theta(\Psi)$, we use *Campbell*'s [1974] expression

$$\theta = \theta_s(\Psi/\Psi_e)^{-1/b} \tag{25b}$$

where Ψ_e is the air entry potential, θ_s is the saturation water content, and b is a parameter.

It was found [*Pachepsky*, 1989] that the additional water retention ($\delta\theta$) as a result of soil salinity may be represented by a linear function of the excessive thickness (Δ) of HIL in the interlayer spacing of smectite minerals. Thus we can write

$$\delta\theta = \varphi\Delta \tag{25c}$$

where the slope value φ depends on the matric potential value. We will regard this as a function:

$$\varphi(\Psi) = \begin{cases} 0 & \Psi \geq \Psi_e \\ \varphi_m \exp[-\omega(pF - pF_m)^2] & \Psi < \Psi_e \end{cases} \tag{25d}$$

where $pF = \log|\Psi|$, Ψ is in centimeters, φ_m is the value of φ for $pF = pF_m$, pF_m and ω are constant (for a given type of soil) parameters which can be found by fitting (25c) and (25d) to the experimental data. An example of experimental data of additional water retention as a function of Δ for coarse loam soil and its fitting by (25c) and (25d) is presented in Figure 1. Actually, the additional water is retained also when $\psi \geq \Psi_e$, yet we set it equal to zero, because of the assumption of the undeformabilty of a solid matrix.

The excessive thickness, Δ, of HIL can be calculated [*Pachepsky*, 1989] to read

$$\Delta = Y_{Na}(12/I^{0.37} - 5), \text{ Å} \tag{25e}$$

where Y_{Na} is the proportion of Na^+ in the total amount of exchangeable cations, and I is the ionic strength of the soil solution.

Combining (25b) and (25c) we obtain

$$\theta = \theta_s(\Psi/\Psi_e)^{-1/b} + \varphi\Delta \tag{25f}$$

In order to characterize the hydraulic conductivity of soil, we use the formula [*Campbell*, 1974]

$$K(\theta) = K_s(\theta/\theta_s)^{2b+3} \tag{26a}$$

where K_s is the saturated hydraulic conductivity.

For the temperature effect on saturated hydraulic conductivity we follow *Milly* [1982]:

$$K_s(T) = K_0 v(T_0)/v(T) \tag{26b}$$

where K_0 is the value of K_s at T_0, and v is the kinematic viscosity.

The K_s variations, affected by soil salinity, can be described as a function of the product $\chi \equiv \Delta I^m$ [*Pachepsky*, 1989], where m is a constant (for a given type of soil) parameter. We will regard this as a function:

$$\frac{K_s}{K_0} \equiv F(\chi) = \begin{cases} 1 & \chi \le \chi^* \\ \exp(\chi^* - \chi) & \chi > \chi^* \end{cases} \tag{26c}$$

where β is a constant parameter, and χ^* is the threshold value of χ. The β and χ^* can be found by fitting (26c) to the experimental data. An example of experimental data of K_s reduction for sandy loam soil [*McNeal and Coleman*, 1966] and its fitting by (26c) is presented in Figure 2.

Combining (26b) and (26c), we obtain

$$K_s(T, \chi) = K_0 F(\chi) v(T_0)/v(T) \tag{26d}$$

We will use (25c), (25d), and (26c) to describe the effect of soil salinity on the soil hydraulic parameters. In general, a more rigorous theoretical approach [e.g., *Russo*, 1988] may be applied. However, it will require more computational efforts. We relax our criteria for some aspects but include more complicated boundary layer computations.

The thermal liquid effect is the least important. Neglecting it, leads to errors in computed evaporation in the order of 1% [*Milly*, 1984]; hence we assume $D_{Tl} = 0$.

Vapor conductivity, $D_{\psi v}$, and the diffusion coefficient for vapor transport due to temperature gradients, D_{Tv}, are given by *Milly* [1984]:

$$D_{\psi v} = \frac{1}{\rho_l} D_{va} \Gamma (n - \theta) \frac{\partial \rho_v}{\partial \psi} \tag{27a}$$

$$D_{Tv} = \frac{1}{\rho_l} D_{va} f' \zeta \frac{\partial \rho_v}{\partial T} \tag{27b}$$

where $D_{va} = 0.229(T/273)^{1.75}$ is the molecular diffusivity ($cm^2\ s^{-1}$) of water vapor in the air [*Kimball et al.*, 1976], $\Gamma = (n - \theta)^{2/3}$ is the tortuosity of the air-filled pore domain [*Lai et al.*, 1976], ζ is the ratio of the average temperature gradient in the air to the overall average temperature gradient, and f' is an enhancement factor [*Milly*, 1984].

The osmotic pressure can be estimated from Vant Hoff's law:

$$P_{os} = \phi RT \sum_i C_i \tag{28}$$

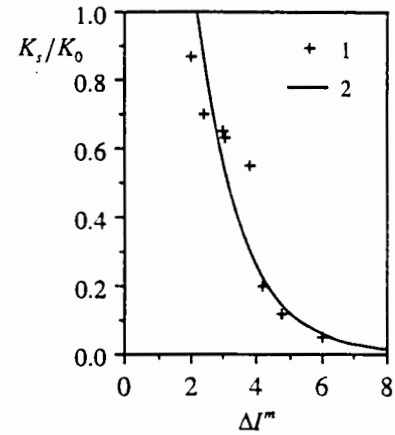

Figure 2. Reduced saturated hydraulic conductivity (K_s/K_0) versus the parameter $\chi \equiv \Delta I^m$ for sandy loam soil: 1 denotes experimental data from *McNeal and Coleman* [1966] as presented by *Pachepsky* [1989] and 2 was computed using (26c) for $\chi^* = 2.2$, $\beta = 0.75$, and $m = 0.30$.

where ϕ is the osmotic coefficient of the electrolyte [*Robinson and Stokes*, 1965]. Note that in (28) C_i is the molar concentration of the ith ion in the equilibrium solution.

The osmotic efficiency coefficient, σ', characterizes the effect of osmotic potential gradients on the water flow. *Bresler* [1973] estimated this coefficient from the diffuse double-layer theory and hydrodynamic considerations. Theoretical σ' values were delineated in graphs in the form $\sigma' \equiv \sigma'(b_l c^{1/2})$ for four monovalent to divalent cationic ratios, where c is the monovalent anion concentration in normality, and $2b_l$ is the water film thickness in Å [*Bresler and Laufer*, 1974]. Macroscopic estimation of this thickness was obtained using *Kemper*'s [1961] formula

$$b_l(\theta) = \left[\frac{3\eta K(\theta)}{\alpha\gamma(L/L_1)\theta\rho_l g}\right] \tag{29}$$

where η is the average dynamic viscosity, and $\alpha\gamma(L/L_1)\theta$ is associated with soil tortuosity. The latter may be replaced by $ae^{10\theta}$, with values for a ranging from 0.005 to 0.001, depending on the surface area of the soil (sandy loam to clay) [*Olsen and Kemper*, 1968; *Bresler et al.*, 1982]. We fitted each of the four σ' theoretical curves by polynomials of a 5th power in order to use them in simulations.

The soil thermal conductivity, λ, is calculated as outlined by *de Vries* [1963]:

$$\lambda = \frac{\theta\lambda_\theta + f_s X_s \lambda_s + f_c X_c \lambda_c + f_a(n - \theta)\lambda_a}{\theta + f_s X_s + f_c X_c + f_a(n - \theta)} \tag{30}$$

where f_s, f_c, and f_a are shape factors of sand, clay and air respectively; λ_s, λ_c, λ_a are their thermal conductivities; and X_s and X_c are volumetric fractions of sand and clay.

The hydrodynamic dispersion coefficient is given by

$$D^* = \tau_c D_m + a_L |q_l^v| \tag{31}$$

where $\tau_c = ae^{10\theta}$ is the soil tortuosity [*Russo*, 1988], D_m is the molecular diffusion coefficient, and λ_L is the longitudinal dispersivity.

5. Numerical Implementation

Implicit finite differences were applied to solve (9) to (11) in vertical direction. Since standard formulation is used, the development of the discrete equations is not presented.

An iterative process was used to solve the set of the nonlinear partial differential and algebraic equations. The solution procedure for each time step is divided into three substeps: (1) solving the nonlinear algebraic equations, (16)–(23), of the low atmosphere boundary layer, (2) solving the nonlinear partial differential equations of water flow (9) and heat transport (10), and (3) solving the nonlinear partial differential equation (11) of salt transport.

Substep 1. To solve (16)–(23), we used the prescribed atmospheric condition data (T_a, q_a, u_a, S_R) and the soil surface condition data (T_s, q_s). The value of T_s is taken as soil temperature at $z = 0$ from the previous time step, or from the previous iteration for every proceeding iteration. The q_s was calculated by $q_s = \rho_{vs}/(\rho_{vs} + \rho_d)$, where ρ_{vs} is the soil vapor density at $z = 0$, and ρ_d is the dry air density. The ρ_{vs} is defined by (3), where values of ψ and P_{os} are taken from the previous time step or from the previous iteration, similar to T_s. The Newton procedure for the system of nonlinear algebraic equations was applied to solve (16)–(23). As a result, we obtained values of the evaporation (E) and the heat (G) fluxes at the soil surface.

Substep 2. The evaluated E and G values were applied to the upper boundary conditions (13) and (14) concerning the water flow (9) and heat transport (10) equations, respectively. A mass conservation scheme, based on the mixed form of the flow equation [*Celia et al.*, 1990], was used for the finite differences discretization of (9). The water flow and heat transport equations were solved simultaneously using the Thomas algorithm in its matrix form. The osmotic pressure head was calculated using concentration values from the previous time step (or previous iteration).

Substep 3. Thereafter the salt transport equation (11) was solved successively for each ion. The Thomas algorithm was used to solve the set of the algebraic equations, resulting from the finite-difference approximation of (11). We tested two different procedures to solve (11):

Procedure 1. At each time step the initial value of the source terms, associated with the ion exchange and the dissolution-precipitation reactions, were set equal to zero. The chemical module LIBRA [*Platonova and Pachepsky*, 1989] was used to bring the solution and the solid phase to chemical equilibrium. Updated values of exchange and solid phase concentrations were then used to calculate source terms in (11). Then a new internal iteration for the transport with a new source term was executed.

Procedure 2. No iteration process between the transport and the chemical module was implemented. Transport equation was solved with zero source terms, and chemical module was called to bring salt components in liquid and on solid phases to chemical equilibrium. A similar algorithm was used by, for example, *Liu and Narasimhan* [1989] and *Simunek and Suarez* [1994].

The results for these two procedures were similar in terms of liquid and solid phase concentrations, as well as evaporation. Hence in all simulations we used the second procedure.

As a result of the three consecutive substeps, we obtain updated values of head, temperature, and concentrations. These are used to calculate new values of ρ_v, P_{os}, and model parameters and to perform a new iteration. The iterative process continues until a desired degree of convergence is obtained for each of the state variables ψ and T.

To test the accuracy, we compared the calculated solutions with known analytical or quasi-analytical solutions of different problems, such as those that describe mutually independent water flow, heat, and solute transport in porous media. Good agreement was obtained. Detailed representation of the numerical behavior of the algorithm is beyond the scope of the present report. However, the performance of the numerical scheme was investigated in terms of its ability to conserve mass of each component, its consistency, convergency, and stability. The scheme was found to be robust, and mass was conserved with a deviation of less than 1% for the flow problem and 3% for the solute transport problem.

Following *Bear et al.* [1991], we exchange the heat transport equation, (10), with a simplified form given by

$$\frac{\partial (c_\lambda T)}{\partial t} = \frac{\partial}{\partial z}\left(\lambda \frac{\partial T}{\partial z} - c_l \mathbf{q}_l T\right) \tag{32}$$

This allows for a reduction in the number of iterations while increasing the time steps. For the considered soil and atmosphere conditions, the maximum differences in the solutions of (10) and (32) did not exceed 2.5%. This difference did not affect the computed evaporation. Hence we used (32) in all simulations.

6. Numerical Simulations

6.1. Comparison With Experimental Data

In order to test the ability of the soil component of the model to predict the transfer processes in soil, we performed simulations using the experimental data of *Nassar and Horton* [1989a] and *Nassar et al.* [1992a]. Full details of the experimental design, the simulation results using steady state and transient water flow, heat, and salt transport models, as well as analysis of the physical processes in the soil columns are given by *Nassar and Horton* [1989a, b, 1992] and *Nassar et al.* [1992a]. A concise description of the salient features is given here for the convenience of the reader.

Laboratory experiments of heat and mass transfer were performed with controlled temperature gradients in sealed columns of silt loam soil with initially uniform water content and solute concentration. The ends of each column were subject to different temperatures to create a temperature gradient. Several soil batches were prepared by mixing soil with different amounts of water and KCl.

In the experiment with horizontally placed columns, the values of the initial water contents, solute concentration, and boundary temperatures were as follows [*Nassar and Horton*, 1989a]: (1) "dry solute-free": water content (volumetric) 0.117, zero initial solute concentration, and constant boundary temperatures of 19.03° and 9.36°C at the hot and cold ends, respectively; (2) "moist solute-free": bulk density 1.09 g/cm^3, initial water content 0.151, zero initial solute concentration, and boundary temperatures of 18.96° and 9.19°C; (3) "dry salinized": bulk density 1.08 g/cm^3, initial water content 0.103, initial solute concentration (molar) 1.111 mol/kg, and boundary temperatures of 19.46° and 9.32°C; and (4) "moist salinized": bulk density 1.04 g/cm^3, initial water content 0.144, initial solute concentration 0.794 mol/kg, and boundary temperatures of 19.02° and 8.93°C. The length of each column

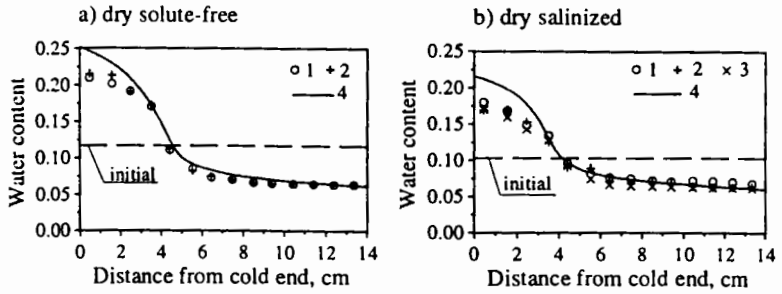

Figure 3. Comparisons of measured and predicted soil water content within (a) dry solute-free and (b) dry salinized horizontal columns: 1, 2, and 3 are experimental replicates [*Nassar and Horton*, 1989a], and 4 is computed.

was 14 cm. A soil water retention curve was determined by using compressed air with fitted glass funnels and a pressure plate apparatus [*Nassar and Horton*, 1989b]. Saturated hydraulic conductivity of the soil was measured in laboratory soil columns, its observed mean value was 0.265×10^{-5} m/s [*Nassar and Horton*, 1989b]. After 31 days (steady state condition), each soil column was sectioned into 1-cm increments to determine the distribution of water content and solute concentration.

In the experiment with a vertically placed column with a length of 10 cm [*Nassar et al.*, 1992a], the initial water content and the KCl concentration of the soil batch were 0.166 and 0.097 mol, respectively. The upper and lower ends were exposed to temperatures 15.09°C and 8.92°C, respectively. The value of saturated hydraulic conductivity of soil was 1.68×10^{-6} m/s. Soil columns were sectioned at 60 and 156 hours after experiment initiation to determine soil water content and solute concentration.

It was found that while water content increased near the cold end, solute concentrations were higher near the hot end of the columns. *Nassar and Horton* [1989a, p. 1329] explained this as "water evaporating from the hotter soil moves as vapor into colder soil, where it condenses and returns as liquid when a favorable gradient of matric and osmotic potential has been established."

Nassar and Horton [1989b] carried out simulations on the basis of a steady state water flow equation with known temperature and solute distribution for the case of horizontally placed columns. A transient model was applied to simulate water and solute distribution in the vertical column *Nassar et al.* [1992]. *Van Genuchten*'s [1980] relation was used to fit experimental water retention curve:

$$\theta = \theta_r + (\theta_s - \theta_r)/[1 + (\alpha_{VG}\Psi)^{n_{VG}}]^{m_{VG}} \qquad (33)$$

where θ_r is irreducible water content; and α_{VG}, n_{VG}, and $m_{VG} = 1 - 1/n_{VG}$ are model parameters. This was then used to find the isothermal liquid diffusivity. Good agreement was obtained between the experiment and the theory [*Nassar and Horton*, 1989b; *Nassar et al.*, 1992a] for "moist solute-free" and "moist salinized" columns.

These experimental data were introduced into our model. For the water flow and solute transport equations, we used a no-flow boundary condition at both ends. Dirichlet boundary conditions were used for the heat transport equation. The gravitation term in the water flow equation was disregarded in the case of horizontal columns. The effect of solute concentration on the soil hydraulic parameters was ignored. Simulations were performed without referring to chemical reactions of ion exchange.

We fitted (33) to the experimental soil water retention curve. Accordingly, the obtained parameters were $\theta_s = 0.65$, $\theta_r = 0.009$, $\alpha_{VG} = 0.0198\ \text{cm}^{-1}$, and $n_{VG} = 1.23$. In the simulations we used an averaged osmotic coefficient of electrolyte value $\phi = 0.9$ [*Robinson and Stokes*, 1965]. The longitudinal dispersivity, a_L, was changed in the range of 0.01 to 1 cm. The model has low sensitivity concerning this parameter for the considered conditions.

Figure 3 shows the observed and predicted water content for dry solute-free and dry salinized horizontal columns. We note a good agreement everywhere, except the region in the vicinity of the cold end with the high water content. When comparing the total water content in the column (area under the water content curve), we found that the computed one is greater than the experimental one. However, the computed mass balance error in these simulations did not exceed 0.03%. This could

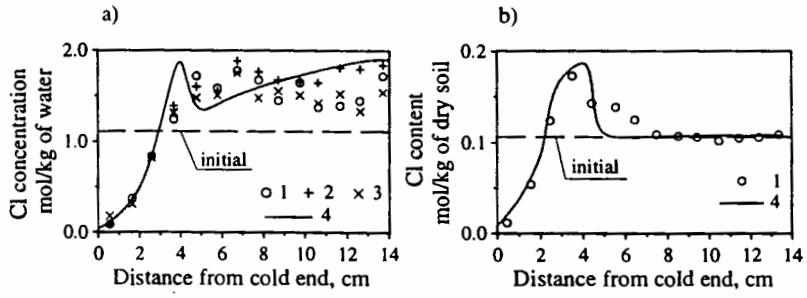

Figure 4. Comparisons of measured and predicted (a) Cl concentration and (b) Cl content within the dry salinized horizontal column: 1, 2, and 3 are experimental replicates [*Nassar and Horton*, 1989a], and 4 is computed.

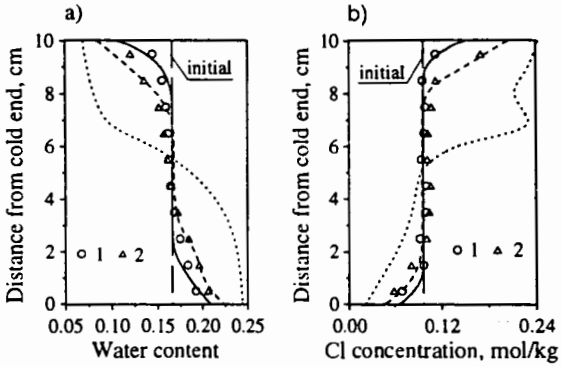

Figure 5. Comparisons of measured and predicted (a) soil water content and (b) Cl concentration within the moist salinized vertical column: 1 and 2 are observed after 60 and 156 hours, respectively [*Nassar and Horton*, 1989a]; solid, dashed, and dotted lines represent the computed values after 60, 156, and 600 hours, respectively.

indicate a small systematic error in the measurements of the water content.

Figure 4 presents the observed and the computed chloride concentrations and their content in the dry salinized column. We note the increase of concentration near the hot end and the appearance of a local maximum value at the vicinity of 4 cm from the hot end. The solute content increases from the cold end to 4 cm, decreases in the 4- to 8-cm range, and then remains relatively constant. Initially, when water content is practically uniform and relatively high, the water in the vapor phase moves towards the cold end. As time evolves, the water content increases near the cold end and decreases near the hot end. This decrease in water content leads to an increase of solute concentration near the hot end of the column; however, the solute content remains constant there (Figure 4). The increase of water content near the cold end allows the movement of water in the liquid phase from cold end to an intermediate point towards the hot end. This yields a local maximum of the concentration.

Table 1. Synthetic Soil Parameters Used in Simulations

	Parameter	Value
	saturated hydraulic conductivity	3.0 cm h^{-1}
	porosity	0.42
	saturation water content	0.42
	density of solid phase	2.65 g cm^{-3}
	air entry potential	−10 cm
	parameter in retention curve formula (25b)	5.0
	paramcter in (25a)	−0.0068°C^{-1}
	parameter in (25d)	0.0012 $Å^{-1}$
	parameter in (25d)	1.9
	parameter in (25d)	2.0
	paramcter for χ calculation in (26c)	0.3
	parameter in (26c)	0.75
	threshold χ value in (26c)	2.2
	longitudinal dispersivity	1.5 cm
	molecular diffusion coefficient	0.05 cm^2 h^{-1}
EC	cation exchange capacity	150 meq kg^{-1}
Na-Ca	selectivity coefficient for Na-Ca exchange	0.15
Na-Mg	selectivity coefficient for Na-Mg exchange	0.25
	emissivity	0.95
	albedo	0.25
	parameter for tortuosity factor calculation	0.003

Figure 5 shows the observed and predicted water content and chloride concentration for the moist salinized vertical column. As in the case of horizontal columns, we observe an increase in the solute concentration near the hot end.

Results indicate the ability of the model to predict, with sufficient accuracy, the water flow and solute transport processes in the closed soil system under temperature gradients. It is interesting to note that the local maximum of the concentration inside the vertical column was not observed experimentally, probably because of the relatively short time of the experiment. Numerical simulation for a longer period (600 hours) demonstrated that this maximum value was formed at a distance of 3 cm from the hot end (Figure 5b).

6.2. Simulation of Evaporation With Synthetic Soil Parameters

To demonstrate the effect of the osmotic pressure gradients on the evaporation, we performed several simulations with synthetic soil (sandy loam) and atmospheric parameters (Tables 1 and 2). All simulations were carried out with constant $z_a = 2$ m and $z_0 = 0.01$ m. The initial temperature distribution in the soil profile was: 20.0°, 26.0°, 27.0°, 26.5°, 25.5°, 24.5°, 23.4°, and 23.3°C at depths of 0, 10, 20, 30, 40, 50, 60, and 100 cm, respectively. The initial matric potential $\psi^0 = -100$ m was constant with depth. The partial CO_2 pressure was set to a constant value of 304 N/m^2. All calculations were carried out for zero initial concentrations of gypsum and calcite.

The problem of water infiltration into sandy loam soil and its subsequent evaporation was considered. The time of infiltration through the soil surface was 3 hours, and the total amount of infiltrated water was 30 mm. The total time interval in each simulation was 5 days. The lower boundary condition, (24), was set at a depth of 1 m.

Simulations were carried out for NaCl and $CaCl_2$ solutions concerning major salt components in soil or for those infiltrating through the surface water. The osmotic coefficient of electrolyte, ϕ, ranges from 0.920 to 0.943 for NaCl and from 0.854 to 1.017 for $CaCl_2$ for concentrations in the range of 0.1 to 1.0 mol/L [*Robinson and Stokes*, 1965]. In our simulations the concentration of these species in the soil solution did not exceed 1 mol/L; hence an average ϕ value of 0.93 was used in all calculations. For each of the two variants (NaCl and $CaCl_2$), two cases were considered: (1) saline soil and nonsaline water (SSNW); that is, initial salt concentration in the soil solution was much higher in compare to the infiltrating water; and (2) nonsaline soil and saline water (NSSW); that is, initial salt concentration in the soil solution was much smaller than that

Table 2. Synthetic Parameters for Atmospheric Conditions Used in the Simulations

Time, h	u_a, m s^{-1}	T_a, °C	q_a	S_R, W m^{-2}
0	0.4	19.7	0.0128	0
3	0.4	19.7	0.0132	0
6	0.7	19.6	0.0151	100
9	0.8	25.6	0.0108	700
12	1.4	29.1	0.0100	900
15	1.5	28.4	0.0104	750
18	0.9	24.4	0.0106	100
21	0.4	21.5	0.0108	0
24	0.4	19.7	0.0128	0

Table 3. Initial and Boundary Ion Concentrations

	NaCl Treatment				$CaCl_2$ Treatment			
	SSNW		NSSW		SSNW		NSSW	
Ion	Soil	Water	Soil	Water	Soil	Water	Soil	Water
Ca^{2+}	10	4	10	4	100	4	10	100
Mg^{2+}	5	1	5	1	5	1	5	1
Na^{+}	100	2	10	100	10	2	10	4
Cl^{-}	100	4	10	100	100	4	10	100
SO_4^{2-}	10	1	10	1	10	1	10	1
HCO_3^{-}	5	2	5	4	5	2	5	4
Total, g/L	6.8	0.4	1.6	6.2	6.5	0.4	1.6	5.9

Initial ion distribution in the soil profile was uniform. Concentrations in meq/L.

of the infiltrating water. The concentration data used in the simulations are presented in Table 3.

The initial calculated osmotic pressure heads ($P_{os}/\rho_l g$) were 27.2 and 4.4 m for the SSNW and NSSW, respectively. In each case, two simulations were carried out: one taking into account the effect of osmotic gradients on the water flow, and another one without considering this effect (osmotic efficiency coefficient, σ', was set equal to zero). The simulation results are shown in Figures 6–10. Note that Figures 7–10 present the results only for NaCl treated soil. The results for all $CaCl_2$ simulations were consistently very similar and therefore are not depicted.

The cumulative computed evaporation as a function of time for the considered cases is presented in Figure 6. The values after 5 days are listed in Table 4. The simulated evaporation rate was controlled by water fluxes in the unsaturated zone (in addition to atmospheric conditions): downward flux beyond the evaporation front and upward flux to the soil surface. These were dependent on temperature, hydraulic, and osmotic pressure gradients.

The postinfiltration moisture distribution profiles were similar for all simulations (Figure 7; after 3 hours). During that time the driving forces associated with the matric and the gravitation potentials were directed downward (Figure 8; after 3 hours). However, the concentration profiles were significantly different when comparing between the SSNW and NSSW cases.

6.2.1. SSNW case. We note that the salt concentration increases with depth (Figure 9; after 3 hours) as nonsaline water infiltrates into the saline soil. The osmotic part of the flow is directed downward and leads to a rise of the total force which drives moisture to the deep soil layers. During the first 24 hours the soil surface dries very quickly (Figure 10a) and the evaporation rate is reduced. During the period of 24 to 120 hours, the salt concentration in the upper 5-cm layer increases, and the osmotic flow changes direction. Yet during this time period the values of the matric potential at the soil surface are very high (from −100 to −13,000 m) and its gradients are very steep (Figure 9). In such conditions the osmotic flux is from 0.1 to 2% of the total one. The evaporation rate is limited by inflow of water from deep soil layers. The direction of the osmotic flux below the upper 5 cm remains downward, reducing this inflow. The osmotic flow is insignificant during all simulation period at the upper 10 cm of soil profile. However, deeper in the profile (15 to 30 cm) its values are ranging from 30 to 90% of the total water flux.

6.2.2. NSSW case. We note that the salt concentration decreases with depth (Figure 9; after 3 hours) when saline water infiltrates into nonsaline soil. The osmotic part of the flux is directed upward lowering the water movement into deeper soil layers. The salt concentration near the soil surface increases considerably with time. Because of the evaporation process, the liquid flow carries salt to the surface which initially has been flushed deeper. These conditions magnify the effect of the osmotic gradients. The water content remains relatively high in the upper 5 cm of the soil (Figures 7 and 10a) during the first 2.5 days. Therefore the temperature at the soil surface during daily hours of the 1st and 2nd days remains relatively low (Figure 10b). Note that the salt concentration at the soil surface increases only during the first 2.5 days (Figure 9), after which it decreases because the downward diffusive flux of the solute exceeds its advective flux to the surface. Simulations results for the period of 12 to 48 hours proves that the osmotic flow shares from 20 to 60% of the total water flux during day hours at the upper 5 cm of the soil profile. During night hours, when evaporation decreases, water content at the soil surface increases (Figure 10a). It induces the oscillations of solute concentration close to the soil surface. It is significant that during nighttime, up to 90% of the total water flux is due to the osmotic pressure gradients. After 48 hours the osmotic flow becomes relatively significant only at depths from 10 to 20 cm. However, its values are rather small (not more than 0.02 mm/h).

7. Discussion

7.1. Comparison Between SSNW and NSSW

Noticing the concentration profiles, we can conclude that the magnitude and the direction of the osmotic flow gradients is

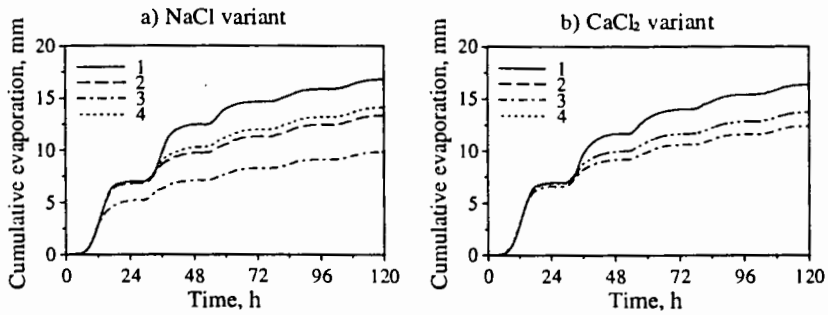

Figure 6. Computed cumulative evaporation: 1 is NSSW with osmosis, 2 is NSSW without osmosis, 3 is SSNW with osmosis, and 4 is SSNW without osmosis.

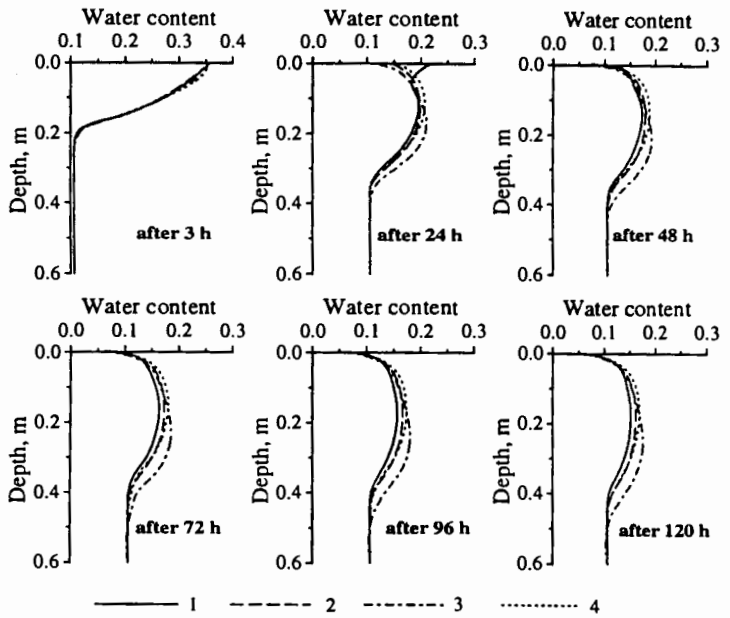

Figure 7. Time evolution of computed water content in soil profile (NaCl variant): 1 is NSSW with osmosis, 2 is NSSW without osmosis, 3 is SSNW with osmosis, and 4 is SSNW without osmosis.

the main reason why the evaporation in the case of NSSW is higher than that of SSNW. Figure 8 demonstrates the evolution of the absolute value of the hydraulic head ($\psi - z$) and the osmotic pressure head in the soil profile. We note that at the postinfiltration period (24 hours) there are zones at depths of 10 to 15 cm, in the case of NSSW, and of 15 to 20 cm in the case of SSNW, where gradients of hydraulic head are relatively low. These zones shift downwards and expand with time. The part of the flow, generated by the hydraulic head, is directed upward and downward above and below these zones, respectively. We also note (Figure 8) that the gradients of the osmotic pressure in these zones are much higher than that of the hydraulic head. Yet in the case of NSSW, the osmotic gradient has upward direction, driving water to the soil surface. In the case of SSNW the direction of the osmotic gradient and its effect are opposite.

7.2. Comparison Between Simulations With Osmosis and Without Osmosis

In the SSNW case osmotic pressure gradients reduces upward water flow to the surface; hence the evaporation obtained by simulation with osmosis is less than that which was obtained without osmosis (Table 4). In the case of NSSW we note the opposite effect. Since NaCl affects the hydraulic properties of

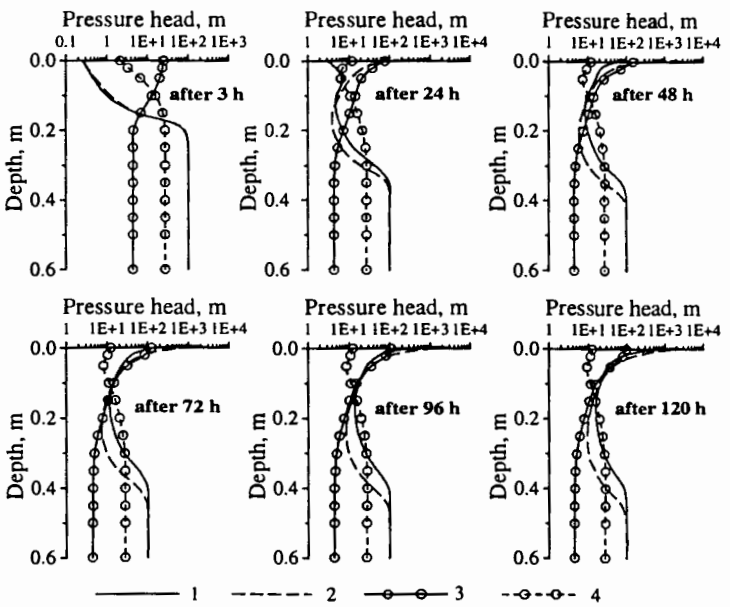

Figure 8. Time evolution of computed hydraulic head (absolute value) and osmotic pressure head in soil profile (NaCl variant with osmosis): 1 and 2 are hydraulic pressure heads for NSSW and SSNW, respectively; 3 and 4 are osmotic pressure heads for NSSW and SSNW, respectively.

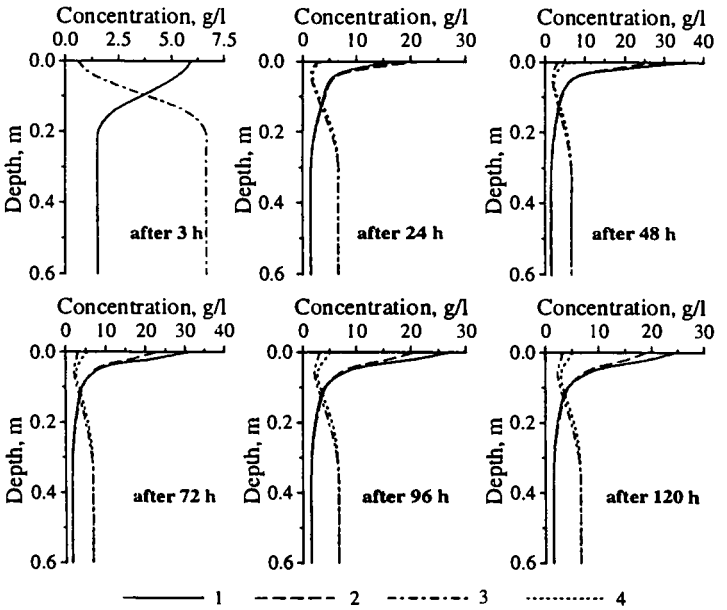

Figure 9. Time evolution of computed salt concentration in soil profile (NaCl variant): 1 is NSSW with osmosis, 2 is NSSW without osmosis, 3 is SSNW with osmosis, and 4 is SSNW without osmosis.

soil, we note that the differences in evaporation between simulations with osmosis and without it are more significant for the NaCl variant.

7.3. Comparison Between Simulations With NaCl and $CaCl_2$

For the NaCl treated soil, initial values of the exchange sodium percent (ESP) were 22 and 2.5% in the SSNW and NSSW cases, respectively. After water infiltration, ESP in the upper 0–2 cm layer decreased to 15% for SSNW. In the case of NSSW it increased to 21%.

For the $CaCl_2$-treated soil, ESP in the soil profile remained less than 1% in all simulations, and the effect of salinity on soil hydraulic properties was negligible. The saturated hydraulic conductivity of soil was greater when compared to the one in which NaCl was the dominant salt, especially for layers close to the soil surface.

When simulating with osmosis, in the case of SSNW, water flow into deep soil layers is increased by osmotic pressure gradients. The soil surface dries very fast for both $CaCl_2$ and NaCl variants. The reverse water flux to the soil surface is more significant for $CaCl_2$, owing to higher hydraulic conductivity resulting with a greater evaporation in than that of NaCl. The evaporation for the latter case (NaCl) is the lowest one (Table 4), since the hydraulic conductivity at the soil surface was considerably diminished owing to high ESP level.

When simulating with osmosis, in the case of NSSW, water flow into deep soil layers is reduced by osmotic pressure gradients. Concerning $CaCl_2$, this downward flux is more significant than that of the NaCl due to a higher hydraulic conductivity. More water is retained by soil close to the surface (Figure 10a), and the evaporation rate is higher regarding NaCl during the first 60 hours (Figure 6). Then, after soil surface dries, the upward water flow for $CaCl_2$ becomes greater and evaporation rate exceeds the one of NaCl. Yet, the total 5 days' evaporation remains somewhat higher for NaCl (Table 4).

When simulating without the osmotic effect, the evaporation value is the same (13.7 mm) for both SSNW and NSSW with $CaCl_2$, since no changes occurred in soil properties. Yet this value is less than the one obtained for NaCl in the case of SSNW (14.2 mm) and higher than in the case of NSSW (13.4 mm). The differences are due to the fact that soil hydraulic

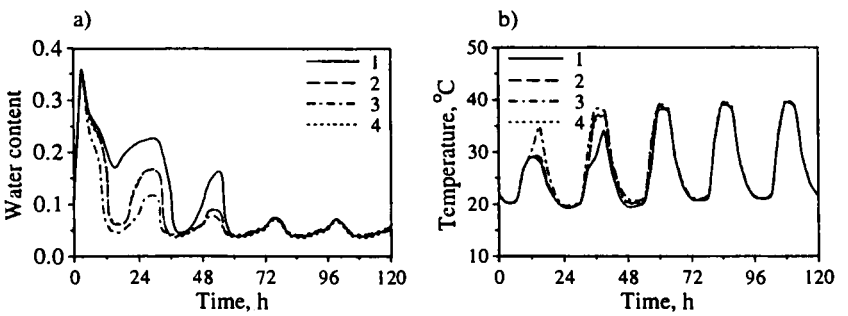

Figure 10. Time evolution of computed (a) water content and (b) temperature at the soil surface (NaCl variant): 1 is NSSW with osmosis, 2 is NSSW without osmosis, 3 is SSNW with osmosis, and 4 is SSNW without osmosis.

Table 4. Computed Cumulative Evaporation for a 5-day Period

Simulation Cases	NaCl Variant		$CaCl_2$ Variant	
	SSNW	NSSW	SSNW	NSSW
With osmosis	9.9	16.9	12.4	16.4
Without osmosis	14.2	13.4	13.7	13.7

Values in millimeters.

conductivity for $CaCl_2$-treated soil is higher. The evaporation in the case of SSNW with $CaCl_2$ is lower, since water which infiltrates below evaporation front becomes unavailable for evaporation. In the case of NSSW with NaCl, the hydraulic conductivity of the upper soil layers is reduced. Hence the evaporation is lower than the one obtained for $CaCl_2$ when osmotic flow is not considered. Note, however, that the differences in evaporation between different cases for simulations without osmosis are minor. Under different soil and atmospheric conditions the correlations between evaporation values can be different.

7.4. Qualitative Comparison With Experimental Data

The obtained results are consistent with the data reported by *Qayyum and Kemper* [1962]. They carried out an experimental study of evaporation from columns (29 cm depth) with Collins clay loam. The upper 10 cm of soil was treated with NaCl or $CaCl_2$ with different concentrations. A mariotte siphon maintained the water table 0.5 cm above the bottom of the columns. The columns were placed under flood lamps to provide "an intensity of incident radiation comparable to that received at mid-day in summer at temperate latitudes" (p. 334). Water loss was measured daily. The values of the average daily losses of water from the NaCl-treated columns were 1.9, 2.8, 2.1, 2.7, and 1.3 mm for the initial NaCl concentration, equal to 0, 0.1, 0.2, 0.4, and 1%, respectively. The increase of evaporation for soils with a salt content of 0.1 to 0.4% in comparison to nonsaline soil was explained by the fact that concentration was not enough to decrease the swelling pressure and reduce the water-transmitting properties to a substantial extent. However, "the increased salt content at the surface was sufficient to help move more water to the surface by a diffusive process" (p. 339). A small decrease of evaporation in the case of 0.2% was associated with the lack of uniformity with which the soil columns were packed. The decrease of evaporation for high salt content (1 and 2%, in another run) was explained by the very high level of concentration near the soil surface which reduced the swelling pressure between clay platelets and consequently the water content. *Qayyum and Kemper* [1962] considered this a cause of considerable decrease in the unsaturated hydraulic conductivity. From their experimental data we note that the average water losses from NaCl-treated column with concentration of 0.1 to 0.4% was 33% higher when compared to water losses from columns without salt.

The lack of details concerning soil properties did not allow us to carry out simulations with data from the *Qayyum and Kemper* [1962] experiments. We therefore make only qualitative comparison of their results with the ones obtained with our model using synthetic soil parameters.

In our simulations the total salt concentration did not exceed 0.05% at the soil surface or 0.1% at a depth of 0.25 m (maximum) in the case of SSNW. In the case of NSSW the salt concentration near the soil surface did not exceed 0.4%. In the case of NSSW for NaCl the total evaporation after 5 days of simulation considering osmotic flow was 26% higher than that with no osmotic effect. Hence our findings are consistent with the experiments of *Qayyum and Kemper* [1962] when considering the NaCl treated columns.

The soil column with 1.0% $CaCl_2$ lost twice as much water than that without salt [*Qayyum and Kemper*, 1962], and the evaporation rate was higher when compared to NaCl-treated column. Our simulations proved that the total evaporation for $CaCl_2$ was less than that of NaCl. This inconsistency may be due the fact that the lower boundary condition was different. In the reported experiment, there was a constant water level at the bottom of the column, that is, continuous supply of water, while in our simulation, the condition (24) allows downward water infiltration through the lower boundary. The hydraulic conductivity of the soil with $CaCl_2$ was higher than that of soil with NaCl. Hence in our simulations water infiltrated deeper and became less available for evaporation. Simulated evaporation rate was higher for NaCl only during the first 60 hours. Thereafter the evaporation rate for $CaCl_2$ treated soil exceeded that of the NaCl.

8. Conclusions

A mathematical model of water flow, heat, and salt transfer in soil was developed. It accounts for the osmotic part of the liquid flow and changes of the hydraulic properties of the soil as a result of its salinity. The flow and heat equations are coupled with the low atmosphere boundary layer model. A numerical algorithm to solve the problem was developed. The soil part of the model was tested with published experimental data of water and solute redistribution under temperature gradients in sealed soil columns.

The numerical modeling of the evaporation from the bare sandy loam soil with synthetic parameters showed that gradients of osmotic potential can play an important role in this process. Simulations were carried out for fully unsaturated soil with no effect on groundwater. In such conditions the computed total evaporation after a 5-day period from nonsaline soil irrigated with saline water (NSSW) from the surface was much higher than that from the saline soil irrigated with nonsaline water (SSNW). In the case of NSSW the osmotic gradients increased water movement to the soil surface as well as evaporation. In the case of SSNW the osmotic pressure gradients reduced water movement to the soil surface and accordingly decreased evaporation. The simulations were consistent with experimental data reported by *Qayyum and Kemper* [1962].

Although the model does not consider the effects such as the changes of albedo, the crust formation during evaporation, and anion exclusion effects, it can serve as a useful tool in understanding the phenomena of evaporation from bare saline soils.

References

Bear, J., J. Bensabat, and A. Nir, Heat and mass transfer in unsaturated porous media at a hot boundary, I, One dimensional analytical model, *Transp. Porous Media*, *6*, 281–298, 1991.

Bresler, E., and A. Laufer, Anion exclusion and coupling effects in nonsteady transport through unsaturated soils, II, Laboratory and numerical experiments, *Soil Sci. Soc. Am. Proc.*, *38*, 213–218, 1974.

Bresler, E., B. L. Mc Neal, and P. L. Carter, *Saline and Sodic Soils: Principles, Dynamics, Modeling*, 236 pp., Springer-Verlag, New York, 1982.

Brutsaert, W., *Evaporation Into the Atmosphere*, D. Reidel, Norwell, Mass., 1982.

Camillo, P. J., and R. J. Gurney, A resistance parameter for bare-soil evaporation models, *Soil Sci.*, *141*(2), 95–105, 1986.

Camillo, P. J., R. J. Gurney, and T. J. Schmugge, A soil and atmospheric boundary layer model for evapotranspiration and soil moisture studies, *Water Resour. Res.*, *19*(2), 371–380, 1983.

Campbell, G. S., A simple method for determining unsaturated conductivity from moisture retention data, *Soil Sci.*, *117*, 311–314, 1974.

Celia, M. A., E. T. Bouloustas, and R. L. Zabra, A general mass-conservative numerical solution for the unsaturated flow equation, *Water Resour. Res.*, *26*(7), 1483–1496, 1990.

Childs, S. W., and C. Malfstaff, Heat and mass transfer in unsaturated porous media, *Final Rep. PNL-4036*, Batelle Pac. Northwest Lab., 1982.

de Silans, A. P., L. Brockler, J. L. Thony, and M. Vauclin, Numerical modeling of coupled heat and water flows during drying in stratified bare soil—comparison with field observations, *J. Hydrol.*, *105*, 109–138, 1989.

de Vries, D. A., Thermal properties of soils, in *Physics of the Plant Environment*, edited by W. R. van Wijk, North-Holland, New York, 1963.

Dufey, J. E., C. M. Petit, Y. Goblet, and H. Laudelout, Modelisation des equilibres physico-chimiques et de la precipitation dans les systemes sol-eau-electrolyte, *Ann. Agron.*, *30*(1), 53–62, 1979.

Edlefson, N. E., and A. B. C. Anderson, Thermodynamics of soil moisture, *Hilgardia*, *15*(2), 31–298, 1943.

Groenvelt, P. H., and B. D. Kay, On the interaction of water and heat transport in frozen and unfrozen soils, II, The liquid phase, *Soil Sci. Soc. Am. Proc.*, *38*(3), 400–404, 1974.

Kemper, W. D., Movement of water as affected by free energy and pressure gradients, I, Application of classic equations for viscous and diffusive movement to the liquid phase in finely porous media, *Soil. Sci. Soc. Am. Proc.*, *25*, 260–265, 1961.

Kimball, B. A., R. D. Jackson, R. J. Rejinato, F. S. Nakayama, and S. Itso, Comparison of field measured and calculated soil-heat fluxes, *Soil. Sci. Soc. Am. Proc.*, *40*(1), 18–25, 1976.

Lai, S. J., M. Tiedje, and A. E. Erickson, In situ measurements of gas diffusion coefficient in soils, *Soil. Sci. Soc. Am. Proc.*, *40*(1), 3–6, 1976.

Letey, J., W. D. Kemper, and L. Noonan, The effect of osmotic pressure gradients on water movement in unsaturated soil, *Soil. Sci. Soc. Am. Proc.*, *33*(1), 15–18, 1969.

Liu, C.-W., and T. N. Narasimhan, Redox-controlled multiple-species reactive chemical transport, 1, Model development, *Water Resour. Res.*, *25*(5), 869–882, 1989.

McNeal, B. L., and N. T. Coleman, Effect of solution composition on soil hydraulic conductivity, *Soil. Sci. Soc. Am. Proc.*, *30*, 308–312, 1966.

Milly, P. C. D., Moisture and heat transport in hysteretic, inhomogeneous porous media: A matric head-based formulation and a numerical model, *Water Resour. Res.*, *18*(3), 489–498, 1982.

Milly, P. C. D., A simulation analysis of thermal effects on evaporation from soil, *Water Resour. Res.*, *20*(3), 1087–1098, 1984.

Nassar, I. N., and R. Horton, Water transport in unsaturated nonisothermal salty soil, I, Experimental results, *Soil. Sci. Soc. Am. J.*, *53*(5), 1323–1329, 1989a.

Nassar, I. N., and R. Horton, Water transport in unsaturated nonisothermal salty soil, II, Theoretical development, *Soil. Sci. Soc. Am. J.*, *53*(5), 1330–1337, 1989b.

Nassar, I. N., and R. Horton, Simultaneous transfer of heat, water, and solute porous media, I, Theoretical development, *Soil. Sci. Soc. Am. J.*, *56*(5), 1350–1356, 1992.

Nassar, I. N., R. Horton, and A. M. Globus, Simultaneous transfer of heat, water, and solute porous media, I, Experiment and analysis, *Soil. Sci. Soc. Am. J.*, *56*(5), 1357–1365, 1992a.

Nassar, I. N., A. M. Globus, and R. Horton, Simultaneous soil heat and water transfer, *Soil. Sci.*, *154*(6), 465–472, 1992b.

Olsen, S. R., and W. D. Kemper, Movement of nutrients to plant roots, *Adv. Agron*, *30*, 91–151, 1968.

Pachepsky, Y. A., Effect of the composition of soil solution and exchange cations on water retention and hydraulic conductivity, *Sov. Soil Sci.*, *4*, 90–103, 1989.

Pachepsky, Y., D. Timlin, B. Acock, H. Lemmon, and A. Trent, 2DSOIL02—A new modular simulator of soil and root processes, 209 pp., Syst. Res. Lab., Agric. Res. Serv., Washington, D. C., 1993.

Philip, J. R., and D. A. de Vries, Moisture movement in porous materials under temperature gradients, *Eos Trans. AGU*, *38*(2), 222–232, 1957.

Pitzer, K. S., *Activity Coefficients in Electrolyte Solutions*, chap. 7, CRC Press, Boca Raton, Fla., 1979.

Platonova, T. K., and Y. A. Pachepsky, Calculation of mass-exchange processes in leached soils, *Sov. Soil Sci.*, *1*, 99–111, 1989.

Qayyum, M. A., and W. D. Kemper, Salt concentration gradients in soils and their effects on moisture movement and evaporation, *Soil Sci.*, *93*, 333–342, 1962.

Robbins, C. W., R. J. Wagenet, and J. J. Jurinak, A combined salt transport-chemical equilibrium model for calcareous and gypsiferous soils, *Soil Sci. Soc. Am. J.*, *44*, 1191–1194, 1980.

Robinson, R. A., and R. H. Stokes, *Electrolyte Solutions*, 571 pp., Butterworths, London, 1965.

Russo, D., Numerical analysis of the nonsteady transport of interacting solutes through unsaturated soil, 1, Homogeneous systems, *Water Resour. Res.*, *24*(2), 271–284, 1988.

Russo, D., and E. Bresler, Soil-water suction relationships as affected by soil solution concentration and composition, in *Agrochemicals in Soils*, edited by A. Banin and U. Kafkafi, pp. 287–297, Pergamon, New York, 1980.

Sasamory, T., A numerical study of atmospheric and soil boundary layers, *J. Atmos. Sci.*, *27*(8), 1122–1137, 1970.

Scanlon, B. R., Evaluation of liquid and vapor water flow in desert soil based on chlorine 36 and tritium tracers and nonisothermal flow simulations, *Water Resour. Res.*, *28*(1), 285–297, 1992.

Scanlon, B. R., and P. C. D. Milly, Water and heat fluxes in desert soils, 2, Nimerical simulations, *Water Resour. Res.*, *30*(3), 721–733, 1994.

Schainberg, I., E. Bresler, and Y. Clausner, Studies on Na/Ca montmorrilonite systems, I, The swelling pressure, *Soil Sci.*, *111*, 214–219, 1971.

Shieldge, J. P., A. B. Kahle, and R. E. Alley, A numerical simulation of soil temperature and moisture variations for a bare field, *Soil Sci.*, *133*(4), 197–207, 1982.

Simunek, J., and D. L. Suarez, Two-dimensional transport model for variably saturated porous media with major ion chemistry, *Water Resour. Res.*, *30*(4), 1115–1133, 1994.

Sophocleous, M., Analysis of water and heat flow in unsaturated-saturated porous media, *Water Resour. Res.*, *15*(5), 1195–1206, 1979.

Van Bavel, C. H. M., and D. Hillel, Calculating potential and actual evaporation from a bare soil surface, *Agric. Meteorol.*, *17*, 453–476, 1976.

van Genuchten, M. T., A closed form equation for predicting the hydraulic conductivity of unsaturated soils, *Soil Sci. Soc. Am. J.*, *44*, 892–898, 1980.

Yeh, G. T., and V. S. Tripathi, A critical evaluation of recent developments in hydrochemical transport models of reactive multichemical components, *Water Resour. Res.*, *25*(1), 93–108, 1989.

P. Berliner, Wyler Laboratory, J. Blaustein Institute for Desert Research, Ben-Gurion University of the Negev, Sede-Boker Campus 84990, Israel.

S. Sorek and A. Yakirevich, Water Resources Research Center, J. Blaustein Institute for Desert Research, Ben-Gurion University of the Negev, Sede-Boker Campus 84990, Israel. (e-mail: alex@hydro.boker.bgu.ac.il)

(Received March 11, 1996; revised November 25, 1996; accepted November 27, 1996.)